# An integral-differential method for impedance determination of the hydrogen oxidation process in the presence of carbon monoxide in the proton exchange membrane fuel cell

K. Darowicki [a], L. Gawel [a], M. Mielniczek [a,*], E. Janicka [a], A. Zielinski [a], J. Mitzel [b], J. Hunger [c]

[a] Department of Electrochemistry, Corrosion and Materials Engineering, Chemical Faculty, Gdansk University of Technology, 11/12 Narutowicza, 80-233, Gdansk, Poland
[b] Institute of Engineering, Thermodynamics, Electrochemical Energy Technology, Pfaffenwaldring 38-40, 70569, Stuttgart, Germany
[c] Zentrum für Sonnenenergie- und Wasserstoff-Forschung Baden-Württemberg (ZSW), Helmholtzstraße 8, 89081, Ulm, Germany

## HIGHLIGHTS

- Methodology for on-line monitoring of fuel cell performance.
- Effects of CO (in the range of 150—300 ppb) pollution of hydrogen stream.
- Determination of anode impedance changes exposed to very low concentrations of CO.
- Novel differential-integral analysis methodology of impedance determination.

## ARTICLE INFO

## ABSTRACT

The impedance of a proton exchange membrane fuel cell powered by hydrogen contaminated with carbon monoxide, ranging from 150 to 300 ppb, is measured and discussed. The tested range of CO concentration complied with the fuel standard specified in the ISO standards. Studies of influence of CO contamination on operation of PEMFC are crucial for further development and commercialization of fuel cells for automotive applications. Based on the measurements made by Dynamic Electrochemical Impedance Spectroscopy (DEIS), changes in the cell impedance as a function of time were determined. An innovative integral-differential methodology for the analysis of chrono-impedance diagrams was developed, which enabled the extraction of the impedance spectra describing the anodic processes. This way of analysis is completely novel and original and it was not presented before in literature. The ability to monitor and diagnose the anode's operation under real operation conditions is demonstrated. The reversibility of the CO adsorption process and the loss of anode catalytic activity were verified. All this issues were not possible to be studied before with the use of classic impedance measurements.

© 2020 Hydrogen Energy Publications LLC. Published by Elsevier Ltd. All rights reserved.

* Corresponding author. Gdańsk University of Technology — Chemistry Faculty, Narutowicza 11/12, 80-233, Gdansk, Poland.
E-mail address: michal.mielniczek@pg.edu.pl (M. Mielniczek).

## Introduction

Proton Exchange Membrane (PEM) fuel cells are already established commercial products. They are most often used as a power source for electric cars [1–3]. Pure hydrogen is the preferred fuel for PEM fuel cells, with the purity of hydrogen fuel being crucial for the proper operation of the fuel cell. Maximum levels of contamination have been determined in the ISO 14687:2019 standard. For carbon monoxide (CO) the limit value is determined to be 0.2 µmol/mol (200 ppb). A significant issue in increasing the demand for fuel cells is the reduction in the cost of hydrogen production, and one way around this issue is to reduce the quality of hydrogen produced [4,5]. It is necessary to be able to thoroughly analyze the impact of individual compounds, which have a negative effect on fuel cell operation. It is worth noting that in the presence of CO, even for concentrations that fall within the ISO standard, the fuel cell performance is significantly reduced.

The performance of PEM fuel cells drops drastically when even a trace amount of carbon monoxide is present in the gaseous fuel [6–10]. The most common techniques utilized to detect CO in hydrogen stream are special sensors [11–15]. However, these sensors do not allow the determination of the impact of CO pollution on the processes occurring in the investigated fuel cell. To be able to obtain information about electrochemical processes occurring inside the cell (in-situ), Electrochemical Impedance Spectroscopy (EIS) is the most often used method [16–23]. However, determining the dynamics of fast processes occurring in the membrane and at the electrodes of an operating fuel cell is difficult for EIS.

For the Hydrogen Oxidation Reaction (HOR), the rate of reaction is much higher than that of Oxygen Reduction Reaction (ORR) [24–26]. This is due to the impedance of the hydrogen oxidation process being negligibly small compared to the ORR impedance [27,28]. However, under certain conditions, one can successfully determine and describe the process dynamics. One of available method to do it is to feed hydrogen both to the anode and cathode of the fuel cell. However, in this case, the impedance of the anode can only be determined during the fuel cell open-circuit voltage, and not under real cell operating conditions [29]. Determining the impedance of the HOR under working conditions is very complicated and are a little-explored research issue [29]. Due to the very fast HOR under standard operating conditions, the obtained spectra of the tested fuel cells are practically equal to the cathode and membrane impedance [18]. This is approach used by many researchers, completely ignoring the anode impedance, considering that approximately the cell impedance is equal to the cathode and membrane impedance. This approach can be found, among others, in the works of Asghari et al. [30], research of O'Rourke et al. [31]. Similar assumptions were adopted by Taghiabadi and Zhian, which were analyzing and discussing degradation on cathode on the basis of cell impedance changes ignoring anodic influence on impedance spectra [32].

There is even more difficulty determining the effect of carbon monoxide on the HOR as a function of time. The first in-situ impedance measurements under galvanostatic conditions showing the effect of CO on the Pt anodic catalyst were completed by Muller et al. [33]. It has been determined that poisoning the anode catalyst causes an increase in the sum of the cell's impedance, with an increase in the overvoltage [34]. Rubio et al. discussed selection of equivalent circuit defining CO poisoning of the anode and importance of impedance values obtained at low frequencies [35]. Many studies have clearly stated that CO only affects the anode. Possible hydrogen crossover to the cathode side may eventually occur after meeting the appropriate conditions. This was discussed by Zhigang et al. in a series of publications where they showed that the CO crossover phenomenon depends on factors such as the concentration of CO in the fuel, the thickness and porosity of the membrane, as well as the pressure difference between the anode and the cathode. In addition, they also found that a well-moisturized membrane minimizes the possibility of CO passing through the membrane [36,37]. Profatilova et al. showed that only with a long period (about 1000 h) of CO flow to the anode a decrease in the cathode active area can be seen [38]. Wagner and Gulzow [39] showed that supplying fuel cell with hydrogen polluted by CO at constant load significantly affects the increase in anode impedance, and the impedance of cathode and membrane can be taken as a constant value. Similarly Tang et al. [40] assumed, that the overpotential caused by CO pollution of hydrogen stream is only caused by anode changes and both cathode and membrane are not affected. Chandesris et al. determined the heterogeneous nature of the effect of CO on the catalyst surface, which also makes it difficult to accurately describe the processes involved [41].

Various new modifications to classic impedance methods are used in fuel cell testing. Becherif et al. conducted tests estimating cell impedance using several frequencies for quick cell diagnostics. The method they developed was based on the projectile motion trajectory, curve fitting and on an estimation based on sinusoidal function [42]. Next research team working under the supervision of Liu proposed a diagnostic method for studying local changes of impedances using special printed circuit boards specially adapted for impedance measurements [43,44]. Suresh and his team have used rapid impedance spectroscopy using dual phase shifted chirp signals connected with simulations for fuel cell diagnostics [45]. It is clear, that use of novel modified impedance methods is crucial for better testing and monitoring of fuel cell operation. Unfortunately methods based on standard EIS are usually limited by time of measurement, which is usually in the range from 30 s to even minutes of measurement, and they cannot be apply to study dynamic processes.

In this work, we present an innovative methodology for identifying and determining the impedance of the anode process, which up to now is an unsolved problem. No previous research has yet determined the time-period needed to poison an anodic catalyst after the introduction of contaminated fuel and with what rate the impedance of the anodic reaction increases. The observation of the evolution of the anode spectrum due to CO pollution has not been determined. The method presented in this work is based on the development of Dynamic Electrochemical Impedance Spectroscopy (DEIS) technique already implemented in the field of fuel cell testing [46–52]. Problem of proper evaluation of CO influence on PEMFC operation is particularly difficult for extremely low

concentrations of CO in gaseous $H_2$. Typically, the effect of CO on the HOR is tested over a concentration range greater than 10 ppm, which is beyond practical importance [53,54]. For these cases, the impedance of the HOR is much greater than the impedance of the membrane and the impedance of ORR. The situation is different when the CO concentration in gaseous hydrogen is extremely low.

For very low concentrations, the process of CO adsorption on the platinum electrode of a PEM cell has not yet been determined by impedance spectroscopy. The biggest advantage of using DEIS is possibility to study object in dynamic conditions. In DEIS method impedance registration is continuous and impedance spectra can be obtained in the time domain. It allowed evaluating CO influence on impedance characteristics over time. With the use of EIS it is not possible to obtain continuous impedance response of the studied object in dynamic conditions. Besides, the implementation of the DEIS technique can give one the ability to detect online the impact of CO and other contaminants. This allows for a quick cleanup reaction to be completed to remove the contaminants. The combination of DEIS methodology and the innovative method for analyzing chrono-impedance diagrams provides completely new information about the processes that were previously impossible to investigate. The differential-integral analysis presented is a completely innovative approach, which perfectly fit for CO adsorption and desorption studies, but can be also with success implemented for different applications.

## Materials and methods

The series of experiments were completed on a single PEMFC constructed by ZSW (Ulm, Germany). MEA, for automotive purposes, with an active surface area of 47 $cm^2$ was used. The working parameters were set and controlled using a ZSW designed fuel cell test bench. The inlet operating parameters were set constant for all experiments. The stack temperature was controlled with a coolant inlet temperature of 70 °C degrees. Humidifiers were heated up to provide 35% relative humidity of the supplied fuel and 60% of supplied oxidant. To avoid water condensation, the gas inlets were preheated to 72 °C degrees. The fuel cell was powered with high purity Hydrogen 5.0 (purity − 99.999%) as the fuel and oil-free compressed air as the oxidant. Hydrogen was fed to fuel cell at a pressure of 1.7 bar in a stoichiometric excess of 1.4. Compressed air was supplied at a pressure of 1.4 bar in stoichiometric excess of 1.6.

Every measurement was performed as follow: cell stabilization was achieved keeping constant parameters for a half-hour before any further experimentation, the addition of CO to hydrogen stream for 2.4 h, and 2.4 h working without CO. Measurements were performed at a current density of $j = 1$ A$cm^2$ at constant operating parameters. The DEIS measurements were performed continuously for 4.8 h during CO adsorption and desorption. Carbon monoxide was added to hydrogen stream in the following concentrations: (a) 0 ppb (b) 150 ppb, (c) 200 ppb, (d) 250 ppb, and (e) 300 ppb. After each measurement, at different concentrations, the fuel cell was shut down and the anode was reactivated. Reactivation is

regular shutdown (by $H_2$-crossover) and cool down to 20 °C, then both electrodes are air-purged with high flow rates (2 A/$cm^2$) for 60 s followed by 20 s $H_2$ flow on the anode.

DEIS testing was completed using a National Instruments (Texas, USA) module equipped with two measurement cards: PXIe-5413 signal generator and a PXIe-4464 for data acquisition. The DEIS measurement and analysis software were written in LabView by the authors. Simultaneously by adding CO to hydrogen stream, multi-sine excitation signal with a total amplitude of 5% of the DC load is applied to the investigated fuel cell. The multi-sine signal is composed of 32 elementary sine waves with a frequency ranging from 3 Hz up to 20 kHz. Detailed mathematical operations and analysis to evaluate impedance spectra are described in the Results and Discussion sections (*vide-infra*, Chrono-impedance of a fuel cell supplied with hydrogen contaminated with carbon monoxide (CO) section).

## Results and discussion

### Chrono-impedance of a fuel cell supplied with clean hydrogen

The chrono-impedance diagram is a set of elementary impedance spectra recorded at equal intervals of time. The chrono-impedance diagram represents a change in cell impedance as a function of time. For comparative and introduction purposes first presented chrono-impedance plot shown in Fig. 1 was registered for fuel cell supplied with hydrogen without presence of CO. All operation conditions were constant and conditions were stationary. There are no visible changes in real and imaginary impedance values and in the shape of spectra. Presented set consist of impedance spectra with two clearly developed impedance semicircles. High frequencies semicircles are directly related to the
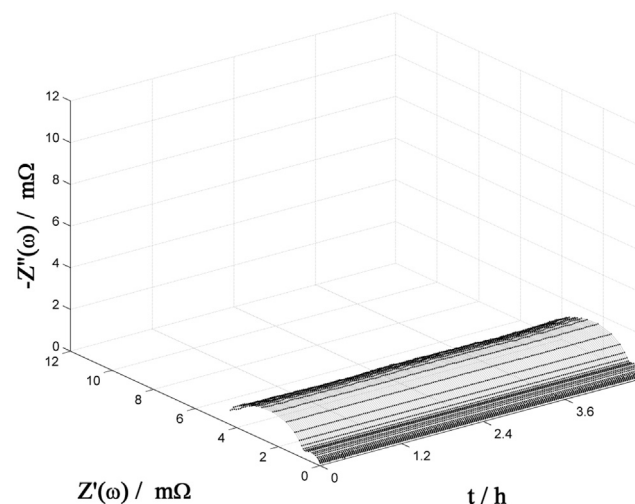


Fig. 1 − A chrono-impedance plot of fuel cell supplied with clean hydrogen with constant operating parameters. Geometric surface area S = 47 $cm^2$, current density $j = 1$ A $cm^{-2}$, measurement frequencies range from 3 Hz to 20 kHz.

membrane impedance. Low frequencies impedance semi-circle, in particular the lowest frequencies range, is associated with the impedance description of ORR.

Use of DEIS methodology shows clearly that stationary conditions occur throughout whole measurement time and indicates that both EIS and DEIS methodology are applicable for this conditions.

### Chrono-impedance of a fuel cell supplied with hydrogen contaminated with carbon monoxide (CO)

Hydrogen contaminated with carbon monoxide, in the following concentrations 150, 200, 250 and 300 ppb, was used in the conducted experiments. Chrono-impedance plots recorded for these CO concentrations are presented in Figs. 2–5. All presented below chrono-impedance plots for all shows that in highest frequencies region, which is usually connected with membrane impedance and in the lowest frequency region, which describes cathodic reaction, no changes are observed. Isofrequency lines of highest and lowest frequencies are parallel to each other, what indicates that there is no change of membrane and cathode impedance. Change of impedance values can be observed in the middle frequency region, which are describing processes connected to CO adsorption and desorption processes. Crucial is fact that presented chrono-impedance show dynamic change of impedance over time. It clearly shows that this experiment cannot be performed by EIS and use of DEIS is necessary to obtain coherent impedance spectra.

Fig. 2 shows a chrono-impedance diagram of a PEM fuel cell powered with hydrogen in the presence of 150 ppb of CO. This change in the impedance value is noticeable. The impedance spectra at the initial time period is in the form of two well-formed semicircles. The second semicircle in the impedance spectra increases with the exposure time of carbon monoxide in the hydrogen stream. In comparison, the first semicircle
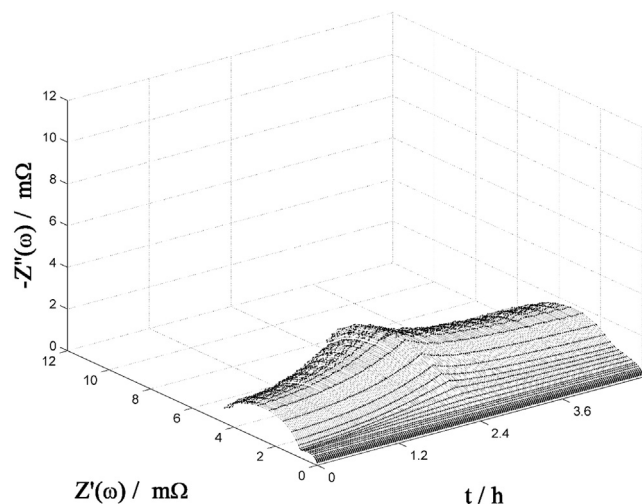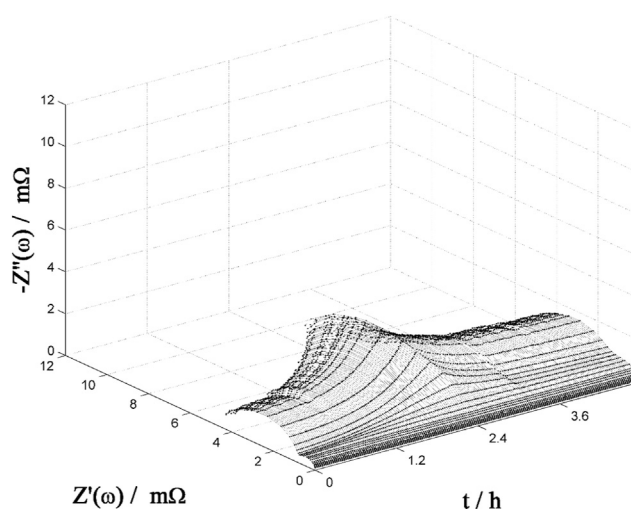


Fig. 3 − A chrono-impedance plot of CO adsorption (up to 2.4 h) and desorption after exposure to 200 ppb of CO in the hydrogen stream. Geometric surface area $S = 47$ cm$^2$, current density $j = 1$ A cm$^{-2}$, measurement frequencies range from 3 Hz to 20 kHz.

does not change as significantly as the second one. After a time of 2.4 h, the fuel cell was supplied with pure hydrogen to observe the desorption of CO. During desroption process impedance values of the second impedance arc decrease over time. The impact of the presence of carbon monoxide on the HOR is more significant at higher CO concentrations.

Fig. 3 shows the chrono-impedance plot with a CO concentration of 200 ppb. The difference between the two semicircles begins to be less noticeable. The impedance of the fuel cell increases by about 1.5 times in comparison to the spectra obtained at the beginning of the experiment. It is worth noting, that a concentration of 200 ppb is acceptable in the ISO
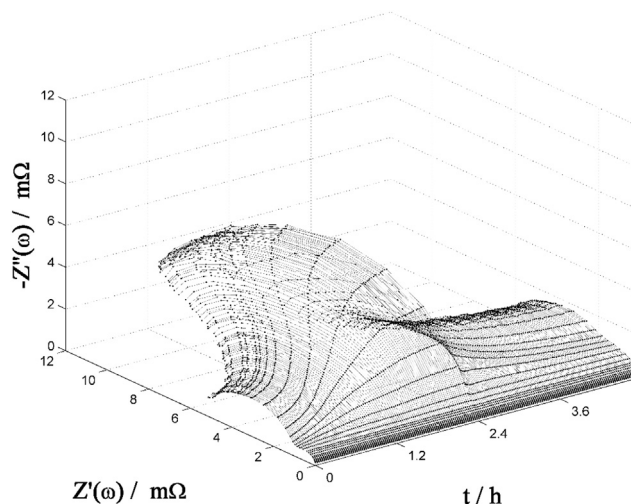


Fig. 2 − A chrono-impedance plot of CO adsorption (up to 2.4 h) and desorption after contamination with 150 ppb CO in the hydrogen stream. Geometric surface area $S = 47$ cm$^2$, current density $j = 1$ A cm$^{-2}$, measurement frequencies range from 3 Hz to 20 kHz.



Fig. 4 − A chrono-impedance plot of CO adsorption (up to 2.4 h) and desorption after exposure to 250 ppb of CO in the hydrogen stream. Geometric surface area $S = 47$ cm$^2$, current density $j = 1$ A cm$^{-2}$, measurement frequencies range from 3 Hz to 20 kHz.
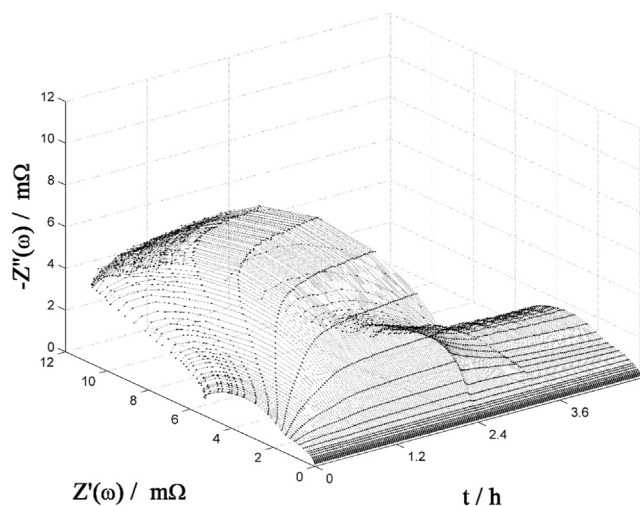
Fig. 5 — A chrono-impedance plot of CO adsorption (up to 2.4 h) and desorption after the exposure of 300 ppb CO in the hydrogen stream. Geometric surface area $S = 47$ cm$^2$, current density $j = 1$ A cm$^{-2}$, measurement frequencies range from 3 Hz to 20 kHz.



Fig. 6 — Voltage changes over time registered simultaneously with DEIS results for all studied concentration of CO.

standards to use as a fuel for automotive application. It is crucial to understand, how this small amount of CO affects the operation of the fuel cell. This effect is even more evident at higher concentration of 250 ppb. The corresponding chrono-impedance diagram is shown in Fig. 4. Over time, the cell impedance increases significantly. Only with increasing the CO concentration in 50 ppb increments, the impedance values between the first spectra and the highest is enlarged by ~2.5 times. The form of the individual impedance spectra also changes. For relatively large time values, the spectra take the form of single semicircles. Similarly to those at lower concentrations, the supply of pure hydrogen causes CO desorption leading to rapid changes in impedance.

The most distinct impact of CO is the change of the fuel cell's impedance is disclosed at a concentration of 300 ppb. These impedance changes over time are observed in Fig. 5. This decrease in impedance is accompanied by a change in the form of the impedance spectra. There is a very rapid increase in the impedance of the fuel cell combined with a change in the form of the impedance spectra. After switching the hydrogen stream from CO to pure hydrogen, CO desorption takes place very quickly. Similarly to a CO concentration of 250 ppb, impedance reduction over time is also accompanied by a change in the form of the individual impedance spectra.

Additionally in Fig. 6 voltage changes results over time for different concentration of CO recorded simultaneously with DEIS are presented. Line marked on the plot at 2.4 h informs about exact moment when CO flows was shut down. Presented voltage characteristics are in perfect agreement with presented above chrono-impedance plots. It is clear that for all CO concentration full reactivation was not observed after 2.4 h of normal operation without CO. Additionally those dependencies clearly shows that all results started for similar value of voltage, what confirms that described in section Materials and methods reactivation procedure was sufficient
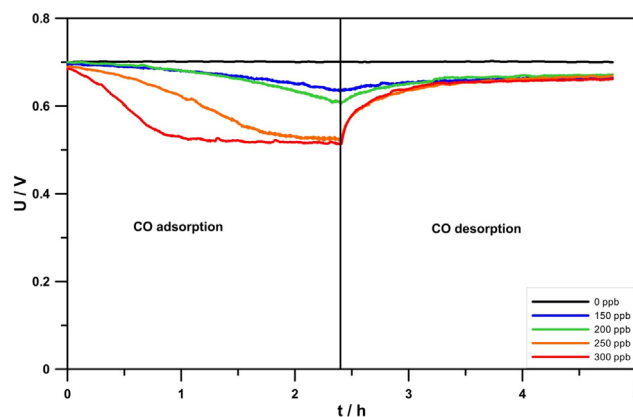
to bring cell back to optimal operation. Moreover, voltage changes clearly indicates that CO in higher concentrations affected not only the size of the changes, but also rate of the changes. It can be clearly observed for voltage changes presented for the highest content of CO. Concentration of 300 ppb of CO caused similar change in the voltage as concentration of 250 ppb, but lowest value was reached much faster.

The changes in impedance spectra under varying CO conditions on the HOR as a function of time is a very significant advancement. However, to assess in detail the effect of carbon monoxide on the HOR, a more detailed analysis is necessary.

### Differential-integral analysis of fuel cell impedance spectra

For EIS measurements, typically the single impedance spectra are available. To properly analyze this, it is necessary to focus on a selection of an equivalent electrical circuit that will accurately reflect the frequency distribution of the spectrum. This methodology works for simple electrode processes. For complex electrode processes, we have to use a complex equivalent electrical circuit, thus making the methodology convoluted. In practice, the complex impedance spectrum can be represented by several different electrical equivalent circuits. This is an ambiguity in the selection of equivalent circuits.

PEM fuel cell impedance is the sum of the impedance of the membrane, cathode and anode, and can be represented with the following equation:

$$Z(j\omega, t) = R_\infty + Z_M(j\omega, t) + Z_C(j\omega, t) + Z_A(j\omega, t) \qquad (1)$$

where $Z(j\omega, t)$ is the fuel cell's impedance, $R_\infty$ is the resistance of an external electrical circuit, $Z_M(j\omega, t)$ is the membrane impedance over time, $Z_C(j\omega, t)$ is the cathode impedance over time, and $Z_A(j\omega, t)$ is the anode impedance over time.

Considering the complexity of the process being investigated which includes the hydrogen oxidation, carbon monoxide adsorption, oxygen reduction, and membrane transport of protons, makes choosing an electrical equivalent circuit a difficult issue. For such complex processes, it is troublesome to find an unambiguous theoretical criterion justifying the layout of the selected circuit. Due to this issue, various

electrical circuits used to analyze the impedance spectra of a PEM fuel cell can be found in the literature [29,55,56]. Selecting the correct circuit is a problematic issue also due to other reasons. The analysis is usually based on a single spectrum. Measurements made by the DEIS method show that the effect of CO on the hydrogen oxidation reaction is not stationary, with the impedance changing over time. And the investigated processes change dynamically. Therefore, impedance spectra determined by the EIS method are not coherent (they are not internally consistent). The selection of an electrical equivalent circuit based on the goal function of $\chi^2$ value is not straightforward. The value of the $\chi^2$ function is a weak criterion that does not explicitly specify the correct selection of an equivalent circuit.

Due to these defined difficulties, it is necessary to develop a new method of analysis that can be used to investigate impedance measurements under non-stationary conditions. This method should eliminate the necessity to select an electrical equivalent circuit, at least for the initial stages of the analysis, where the spectra are made up of a series of complex processes. In the first step, an analysis of the conditions of the experiment is presented. The HOR is studied under galvanostatic conditions. The current load value equals 47 A, which gives a current density of 1 A cm$^{-2}$. It is worth noting that the conditions of the experiment define the impedance of the membrane. Invariability in the time of the current causes the stream of hydrogen protons passing through the membrane from the anode to cathode and is constant. It can, therefore, be assumed that the membrane impedance does not change over time. Also, the stream of gaseous oxygen introduced into the cathode does not change during the experiment. The stream of hydrogen protons flowing through the membrane to the cathode, as previously stated, is constant. The temperature at which the fuel cell was tested is also constant. This preliminary analysis suggests that the impedance of the ORR and the membrane impedance do not change over time.

Hydrogen in the presence of carbon monoxide is fed into the anode reaction space. Therefore, the observed changes in the fuel cell impedance, over time, are identified with the changes in the anode impedance over time. The analysis of the experiment conditions allows us to simplify Eq. (1) to form:

$$Z(j\omega, t) = R_\infty + Z_M(j\omega) + Z_C(j\omega) + Z_A(j\omega, t) \tag{2}$$

where $Z_M(j\omega)$ is the membrane impedance independent of time, and $Z_C(j\omega)$ is the cathode impedance independent of time.

This equation is crucial for this newly developed method of analyzing chrono-impedance diagrams. Individual elementary impedance spectra forming a chrono-impedance diagram are determined at even time interval between subsequent spectra, $h$. This is due to the utilized measurement methodology of the DEIS technique developed by Darowicki et al. [57−60]. Consequently, it is possible to differentiate chrono-impedance diagrams in the time domain.

The values of the differentials for each frequency, $\omega_i$, and time, $t_k$, are determined according to the known relationships (Eqs. (3) and (4)):

$$\frac{Z_A'(\omega_i, (t_k + h)) - Z_A'(\omega_i, t_k)}{h} \approx \left(\frac{dZ_A'(\omega_i, t)}{dt}\right)_{t_k} \tag{3}$$

$$\frac{Z_A^{'}(\omega_i, (t_k + h)) - Z_A''(\omega_i, t_k)}{h} \approx \left(\frac{dZ_A''(\omega_i, t)}{dt}\right)_{t_k} \tag{4}$$

where $Z_A'(\omega_i, t_k)$ is the real part of anode impedance, $Z_A''(\omega_i, t_k)$ is the imaginary part of anode impedance, $t_k$ is time, and $h$ is the time interval.

Differentiation of the chrono-impedance diagrams of the fuel cell results in the elimination of the $Z_C(j\omega)$, $Z_M(j\omega)$ and $R_\infty$ terms from the equation: The obtained chrono-impedance diagrams are determined by the electrochemical parameters of the anodic process:

$$\frac{dZ(j\omega, t)}{dt} \approx \frac{dZ_A(j\omega, t)}{dt} = \frac{dZ_A'(\omega, t)}{dt} + j\frac{dZ_A''(\omega, t)}{dt} \tag{5}$$

Using the described procedure (Eqs. (3)−(5)), differential chrono-impedance diagrams representing the impedance of the anode are obtained.

The transition from differential impedance to impedance (original representation) requires a differential integration operation. For the integration procedure, the same time interval between subsequent spectra, $h$, used in the differentiation operation was maintained. The anode impedance extraction was obtained by integrating differential chrono-impedance diagrams:

$$Z_A'(\omega_i, t) = Z_A'(\omega_i, 0) + \int_0^t \left(\frac{dZ'(\omega_i, t)}{dt}\right) dt \approx Z_A'(\omega_i, 0)$$
$$+ \sum_{k=1}^N \left(\frac{dZ_A'(\omega_i, t_k)}{dt}\right)_{t_k} h \tag{6}$$

$$Z_A''(\omega_i, t) = Z_A''(\omega_i, 0) + \int_0^t \left(\frac{dZ''(\omega_i, t)}{dt}\right) dt \approx Z_A''(\omega_i, 0)$$
$$+ \sum_{k=1}^N \left(\frac{dZ_A^{'}(\omega_i, t_k)}{dt}\right)_{t_k} h \tag{7}$$

Determining the chrono-impedance diagrams of the anode process by digital integration requires the determination of the real impedance part $Z_A'(\omega, 0)$ (Eq. (6)) and the imaginary impedance part $Z_A''(\omega, 0)$ (Eq. (7)) a time zero. However, we know that at zero time there is no carbon monoxide effect on the platinum anode. It is known that the rate of hydrogen oxidation is 2-3 orders of magnitude faster than the rate of oxygen reduction. Consequently, at a time equal to zero, the anode impedance is negligibly small relative to the membrane impedance and the cathode impedance (Eq. (8)). The initial following condition is therefore observed:

For $t = 0$ and for each value of $\omega_i$

$$Z_A'(\omega_i, t_k) \approx 0 \text{ and } Z_A''(\omega_i, t_k) \approx 0 \tag{8}$$

Numerical differentiation of the chrono-impedance

diagrams for measurement frequencies allows for the elimination of constant impedance components. Numerical integration, on the other hand, allows one to reproduce impedance spectra after eliminating the constant components.

### The impedance of HOR of a fuel cell supplied with clean hydrogen

Integration of the numerical differential chrono-impedance diagrams is a mathematical procedure giving primary relationships. Integral-differential analysis of chrono-impedance plot from Fig. 1 was performed to shows correctness of proposed integral-differential analysis procedure. Therefore, chrono-impedance plot presented in Fig. 1 was subjected to differentiation, what was followed by integration. Obtained results presented in Fig. 7 confirm stationary condition of investigated process. Changes of imaginary and real part of impedance results from measurement errors.

Thanks to obtaining presented relation (Fig. 7.) measurement relative error can be easily determined. Changes of imaginary and relative impedance for every frequency were divided by module of impedance, what allows determining uncertainty of performed analysis. Obtained relations presented in Fig. 8 shows that relative error for most frequencies were lower than 1%. The highest values of relative error were obtained for highest frequencies, what is connected with very low value of impedance module.

### The impedance of HOR of a fuel cell supplied with hydrogen contaminated with carbon monoxide (CO)

For all studied concentration differential-integral analysis were performed and results are presented in Figs. 9–12. As results of this analysis anode chrono-impedance diagrams were obtained. Membrane and cathode impedance were filtered out using numerical differentiation and integration operations.
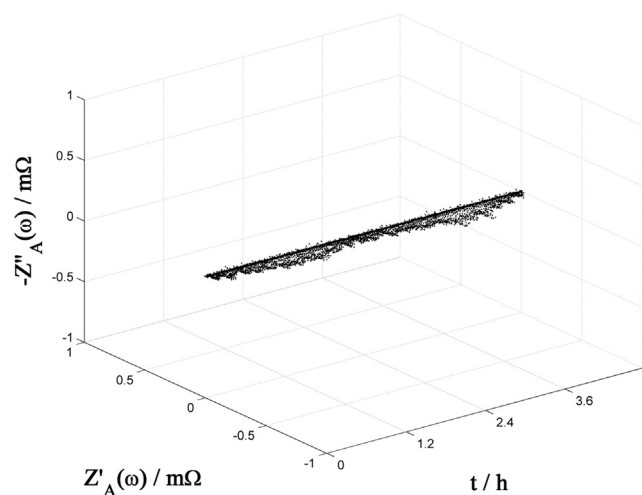
Anode impedance for the lowest studied concentration is shown in Fig. 9. Over time, the impedance increases successively to obtain a maximum value at a time of 2.4 h. After this time, pure hydrogen is fed to the anode and a monotonic impedance drop is observed.

Over the studied frequency range, all elementary impedance spectra have the form of two semicircles. For the initial time period, which is termed the adsorption time, an increase in both the high-frequency and low-frequency semicircles is observed. Impedance of anode reaches quite significant value in relation to impedance of the cell. It is important to notice, that even very small increase of CO concentration is greatly affecting anode operation. During desorption, a decrease in the size of both semicircles is observed.

The carbon monoxide adsorption process is a non-faradaic process. However, this process affects the HOR. The observation of two semicircles is indicative of a two-stage hydrogen oxidation process.

An increase in the carbon monoxide content to a concentration of 200 ppb causes even greater changes in the size of the anode impedance, which can be observed in Fig. 10. An increase in the carbon monoxide content increases the resistance to hydrogen oxidation. A CO concentration of 200 ppb in the hydrogen is enough to increase the anode impedance by several times. This has a significant influence on the fuel cell's efficiency. During the adsorption period, two capacitive semicircles are visible. These semicircles expand in time. During the desorption, two semicircles are also observed.

A further increase in the concentration of CO in hydrogen should cause even greater changes in the impedance of the hydrogen oxidation process. Fig. 11 shows the chrono-impedance diagrams of hydrogen oxidation in the presence of 250 ppb carbon monoxide.

With 250 ppb CO contamination, the impedance changes are even more discernible than for concentration of 200 ppb. The HOR impedance increases rapidly over time. Moreover, a significant difference in the shape of elementary impedance spectra is visible. The size of the high-frequency semicircle increases more than that of the low-frequency one. Increasing the CO content in hydrogen is more likely to affect the high-frequency half-period. Only one semicircle is visible for the highest concentrations of CO. After switching the anode stream to pure hydrogen, the impedance drops rapidly due to CO desorption. The observed changes, in the form of impedance spectra, are caused by the impact of carbon monoxide on the HOR. The observed effects are the most visible in the chrono-impedance diagrams determined for a 300 ppb CO concentration shown in Fig. 12.

Individual impedance spectra forming a chrono-impedance diagram are also in the form of two capacitive semicircles. In this case, the low-frequency semicircle is much less expanded than seen for lower CO contents. For larger exposure times, low-frequency impedance arcs are very poorly developed comparing to relatively large high-frequency semicircles. Within the range of times corresponding to CO desorption process, a sharp decrease in the impedance value is visible over time.



Fig. 7 – A chrono-impedance plot presented in Fig. 1 after differential-integral analysis. Geometric surface area $S = 47$ cm$^2$, current density $j = 1$ A cm$^{-2}$, measurement frequencies range from 3 Hz to 20 kHz.
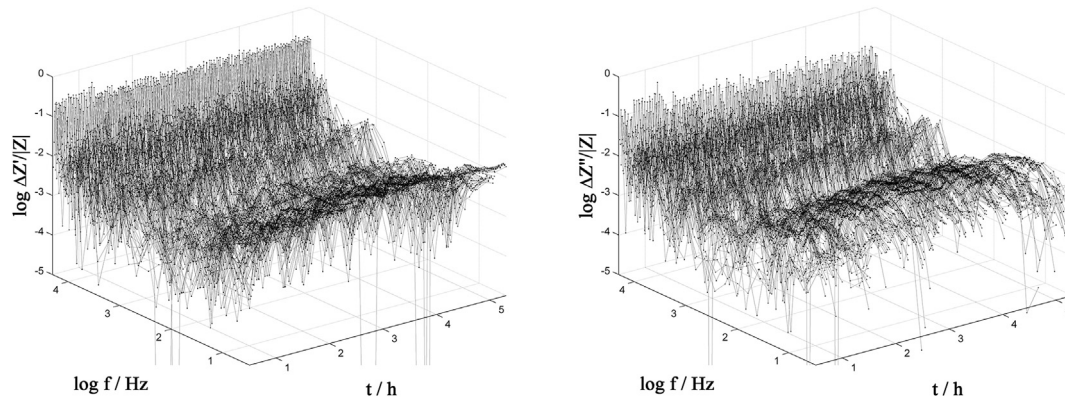
Fig. 8 – Relative error of real and imaginary change of impedance determined for chrono-impedance presented in Fig. 1.
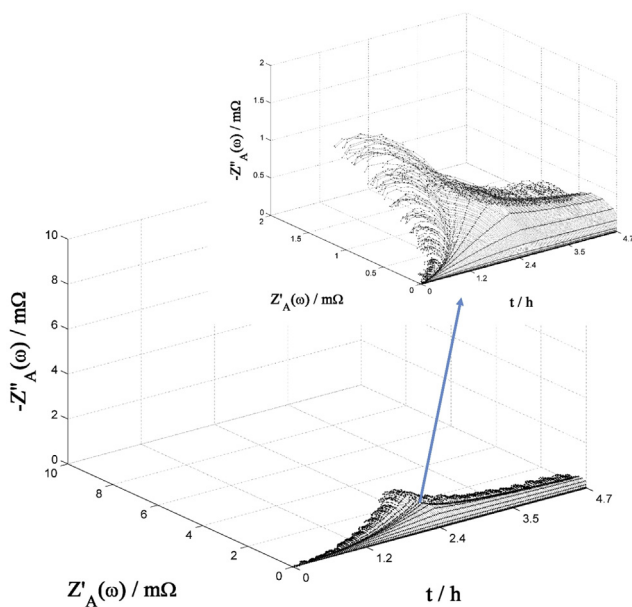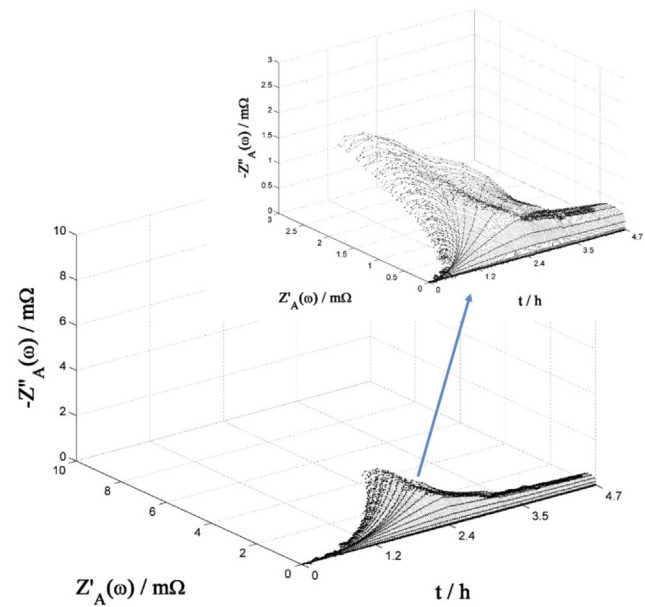


Fig. 9 – A chrono-impedance plot after differential-integral analysis of CO adsorption (up to 2.4 h) and desorption after exposure of 150 ppb CO in the hydrogen stream. Geometric surface area S = 47 cm², current density j = 1 A cm⁻², measurement frequencies range from 3 Hz to 20 kHz.

Fig. 10 – A chrono-impedance plot after differential-integral analysis of CO adsorption (up to 2.4 h) and desorption after exposure of 200 ppb CO in the hydrogen stream. Geometric surface area S = 47 cm², current density j = 1 A cm⁻², measurement frequencies range from 3 Hz to 20 kHz.
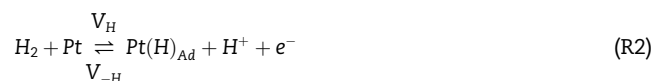
Even at the lowest CO concentration of 150 ppb, the anode impedance increases monotonically over time. The chrono-impedance diagram for a CO content of 200 ppb show the analogical course but with more severe changes. The most significant changes in the impedance of the hydrogen oxidation reaction are visible on the chrono-impedance diagrams with carbon monoxide concentrations at 250 ppb and 300 ppb. Changes in the impedance over time are associated with carbon monoxide adsorption.

CO adsorption on Pt is non-faradaic process, which is decreasing numbers of active centers of Pt and it is described by following reaction (R1):

$$CO + Pt = Pt(CO)_{Ad} \tag{R1}$$

Based on above it can be assumed that adsorption of carbon monoxide does not affect mechanism of anodic reaction.

According to the theoretical description presented by Armstrong [61,62], two capacitive semicircles are observed when a two-stage electrochemical reaction takes place with an adsorbing intermediate. HOR according to the Heyrovsky-Volmer mechanism occurs as follow (R2-R3):

$$H_2 + Pt \underset{V_{-H}}{\overset{V_H}{\rightleftharpoons}} Pt(H)_{Ad} + H^+ + e^- \tag{R2}$$

$$Pt(H)_{Ad} \underset{V_{-V}}{\overset{V_V}{\rightleftharpoons}} Pt + H^+ + e^- \tag{R3}$$

Our observed results fit accurately into the theoretical description of the electrode impedance presented by Armstrong.
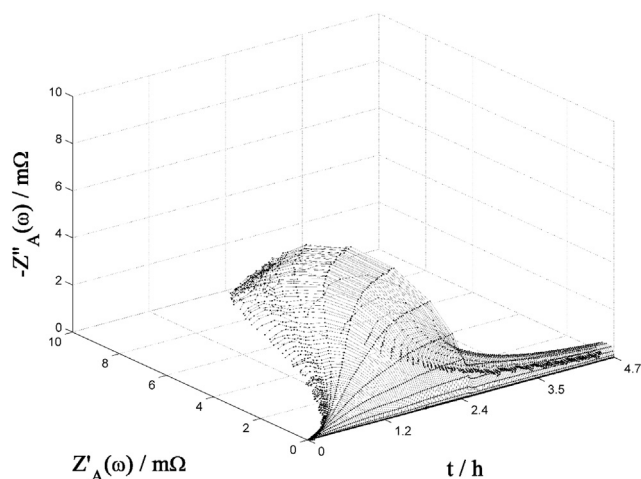
**Fig. 11 – A chrono-impedance plot after differential-integral analysis of CO adsorption (up to 2.4 h) and desorption after exposure of 250 ppb CO in the hydrogen stream. Geometric surface area S = 47 cm², current density j = 1 A cm⁻², measurement frequencies range from 3 Hz to 20 kHz.**
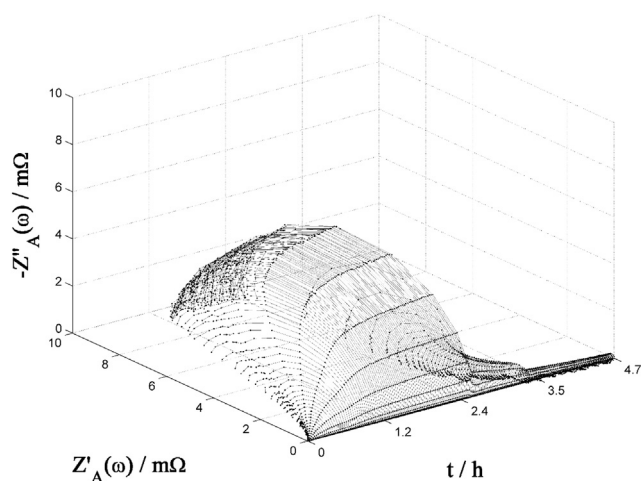


**Fig. 12 – A chrono-impedance plot after differential-integral analysis of CO adsorption (up to 2.4 h) and desorption after exposure of 300 ppb CO in the hydrogen stream. Geometric surface area S = 47 cm², current density j = 1 A cm⁻², measurement frequencies range from 3 Hz to 20 kHz.**

A detailed theoretical analysis of the HOR was carried out by Kucernak and Zalitis [63]. In their work, full derivations of the Heyrovsky-Volmer, Tafel-Volmer and Heyrovsky-Tafel-Volmer mechanisms under steady-state conditions were performed. Only the Heyrovsky-Volmer mechanism was influenced by pH.

Wang et al. has shown that the process of hydrogen oxidation can proceed in two ways depending on the over-potential value [64,65]. Wang's research has shown that for low currents (HOR overpotential of less than 50 mV) the hydrogen oxidation reaction proceeds according to the Tafel-Volmer model. For high currents (HOR overpotential greater

than 50 mV), hydrogen oxidation occurs according to the Heyrovsky-Volmer mechanism. Wang's research suggests that for low currents (hydrogen oxidation reaction over-potential of less than 50 mV) the hydrogen oxidation reaction proceeds according to the Tafel-Volmer model. For high currents (hydrogen oxidation reaction overpotential of greater than 50 mV), hydrogen oxidation is carried out according to the Heyrovsky-Volmer mechanism. The experimental results presented in this paper are consistent with the results of theoretical analyzes by Wang [64,65], Kucernak and Zalitis [63]. The used of DEIS methodology and new proposed integral-differential analysis of spectrum gives a more detailed insight of CO adsorption process and gives possibility to better understanding PEMFC behavior affected by CO. It was clearly proven that even small trace of CO in fuel cells, which is accepted by ISO standards, significantly, affects PEMFC operation. This fact was confirmed by both voltage monitoring and DEIS results, which were performed simultaneously. Additionally it was found out that these changes are not reversible in short time during normal operation. Shutdown with reactivation procedure was necessary to bring cell to optimal performance. Proposed integral-differential analysis was confirmed as very useful tool, which can simplify impedance analysis and can be with success used for different applications.

## Conclusions

Adsorption of carbon monoxide at extremely low concentrations (150–300 ppb) affects the fuel cell impedance. Even for extremely low concentrations of CO, which meet the requirements of ISO 14687:2019 standards, fuel cell operation is significantly affected. Changes in the impedance of the entire cell are caused by changes in the impedance of the HOR which is affected by carbon monoxide. This process is non-stationary. For this reason, the impedance spectra obtained by EIS are internally inconsistent. Their precise analysis due to the complexity and non-stationary nature of the processes taking place is questionable. Impedance measurements made using DEIS give satisfactory and reliable results. This technique makes it possible to track changes in the fuel cell impedance during online operation. The measured impedance of the entire cell is the sum of the impedance of ORR, the impedance of HOR, and the impedance of the membrane. A method for extracting the anode impedance has always been an ambiguous matter. Here, a novel developed differential-integral method for analysis is an effective way to extract anode impedance. In this method, the membrane impedance and cathode impedance can be easily separated from the anode impedance, due to their stability under experimental conditions.

The presented chrono-impedance diagrams of the hydrogen oxidation reaction in the presence of carbon monoxide illustrate the non-uniformity of the studied process. For all the tested concentrations of CO in H₂, elementary impedance spectra have the form of two capacitive semicircles. These spectra evolve over time. A clear increase in the impedance is visible. The two observed semicircles confirm that the hydrogen oxidation process on a platinum electrode

is a two-step process. The first stage is the Heyrovsky reaction leading to the formation of an adsorbed intermediate. The second stage is the oxidation of the adsorbed intermediate to a hydrogen cation. These observations are consistent with previously discussed theoretical analyzes. Changes in the charge transfer resistance of the HOR allow the determination of changes in the electrocatalytic efficiency of the anode over time. The observation of anode impedance changes after switching the stream of polluted hydrogen to pure hydrogen allows for the determination of the dynamics of the carbon monoxide desorption process. For the desorption process time, successive reduction of impedance is observed. For the low concentration range, CO adsorption is reversible. The proposed DEIS measuring technique is an efficient tool that allows you to monitor changes in the fuel cell under operating conditions. The developed differential-integral analysis method is an effective tool for analyzing chrono-impedance diagrams with non-stationary processes.

## Declaration of competing interest

The authors declare that they have no known competing financial interests or personal relationships that could have appeared to influence the work reported in the paper.

## Acknowledgements

## Appendix A. Supplementary data

Supplementary data to this article can be found online at https://doi.org/10.1016/j.ijhydene.2020.07.038.

REFERENCES

[1] Fuel-cell cars finally drive off the lot. C&EN Global Enterp 2017;95:28–32. https://doi.org/10.1021/cen-09538-cover.
[2] Ahmadi P, Torabi SH, Afsaneh H, Sadegheih Y, Ganjehsarabi H, Ashjaee M. The effects of driving patterns and PEM fuel cell degradation on the lifecycle assessment of hydrogen fuel cell vehicles. Int J Hydrogen Energy 2020;45:3595–608. https://doi.org/10.1016/j.ijhydene.2019.01.165.
[3] Lohse-Busch H, Stutenberg K, Duoba M, Liu X, Elgowainy A, Wang M, Wallner T, Richard B, Christenson M. Automotive fuel cell stack and system efficiency and fuel consumption based on vehicle testing on a chassis dynamometer at minus 18 °C to positive 35 °C temperatures. Int J Hydrogen Energy 2020;45:861–72. https://doi.org/10.1016/j.ijhydene.2019.10.150.
[4] Bacquart T, Arrhenius K, Persijn S, Rojo A, Auprêtre F, Gozlan B, Moore N, Morris A, Fischer A, Murugan A, Bartlett S, Doucet G, Laridant F, Gernot E, Fernández TE, Gómez C, Carré M, De Reals G, Haloua F. Hydrogen fuel quality from two main production processes: steam methane reforming and proton exchange membrane water electrolysis. J Power Sources 2019;444:227170. https://doi.org/10.1016/j.jpowsour.2019.227170.
[5] Chugh S, Meenakshi S, Sonkar K, Sharma A, Kapur GS, Ramakumar SSV. Performance evaluation of PEM fuel cell stack on hydrogen produced in the oil refinery. Int J Hydrogen Energy 2020;45:5491–500. https://doi.org/10.1016/j.ijhydene.2019.06.160.
[6] Baschuk JJ, Li X. Carbon monoxide poisoning of proton exchange membrane fuel cells. Int J Energy Res 2001;25:695–713. https://doi.org/10.1002/er.713.
[7] Springer TE, Rockward T, Zawodzinski TA, Gottesfeld S. Model for polymer electrolyte fuel cell operation on reformate feed: effects of CO, H[sub 2] dilution, and high fuel utilization. J Electrochem Soc 2001;148:A11. https://doi.org/10.1149/1.1344516.
[8] Wang W, Wang W, Chen S. The effects of hydrogen dilution, carbon monoxide poisoning for a Pt–Ru anode in a proton exchange membrane fuel cell. Int J Hydrogen Energy 2016;41:20680–92. https://doi.org/10.1016/j.ijhydene.2016.09.151.
[9] Kheradmandinia S, Khandan N, Eikani MH. Two-layer anode electrode with non-noble catalysts as CO tolerant structure for PEM fuel cell. Int J Hydrogen Energy 2019. https://doi.org/10.1016/j.ijhydene.2019.09.031.
[10] Wong CY, Wong WY, Ramya K, Khalid M, Loh KS, Daud WRW, Lim KL, Walvekar R, Kadhum AAH. Additives in proton exchange membranes for low- and high-temperature fuel cell applications: a review. Int J Hydrogen Energy 2019;44:6116–35. https://doi.org/10.1016/j.ijhydene.2019.01.084.
[11] Tournier G, Pijolat C. Influence of oxygen concentration in the carrier gas on the response of tin dioxide sensor under hydrogen and methane. Sensor Actuator B Chem 1999;61:43–50. https://doi.org/10.1016/S0925-4005(99)00278-6.
[12] Wurzinger O, Reinhardt G. CO-sensing properties of doped SnO2 sensors in H2-rich gases. Sensor Actuator B Chem 2004;103:104–10. https://doi.org/10.1016/j.snb.2004.04.041.
[13] Prasad RM, Gurlo A, Riedel R, Hübner M, Barsan N, Weimar U. Microporous ceramic coated SnO2 sensors for hydrogen and carbon monoxide sensing in harsh reducing conditions. Sensor Actuator B Chem 2010;149:105–9. https://doi.org/10.1016/j.snb.2010.06.016.
[14] Min Jeffery, Kim Jung. Electrochemical analysis for demonstrating CO tolerance of catalysts in polymer electrolyte membrane fuel cells. Nanomaterials 2019;9:1425. https://doi.org/10.3390/nano9101425.
[15] Korotcenkov G, Han SD, Stetter JR. Review of electrochemical hydrogen sensors. Chem Rev 2009;109:1402–33. https://doi.org/10.1021/cr800339k.
[16] Giner-Sanz JJ, Ortega EM, Pérez-Herranz V. Mechanistic equivalent circuit modelling of a commercial polymer electrolyte membrane fuel cell. J Power Sources 2018;379:328–37. https://doi.org/10.1016/j.jpowsour.2018.01.066.
[17] Yuan X, Wang H, Colinsun J, Zhang J. AC impedance technique in PEM fuel cell diagnosis—a review. Int J Hydrogen Energy 2007;32:4365–80. https://doi.org/10.1016/j.ijhydene.2007.05.036.
[18] Wu J, Yuan X, Wang H, Blanco M, Martin J, Zhang J. Diagnostic tools in PEM fuel cell research: Part I

Electrochemical techniques. Int J Hydrogen Energy 2008;33:1735–46. https://doi.org/10.1016/j.ijhydene.2008.01.013.

[19] Pivac I, Barbir F. Inductive phenomena at low frequencies in impedance spectra of proton exchange membrane fuel cells – a review. J Power Sources 2016;326:112–9. https://doi.org/10.1016/j.jpowsour.2016.06.119.

[20] Mitzel J, Sanchez-Monreal J, Garcia-Sanchez D, Gazdzicki P, Schulze M, Häußler F, et al. Fault diagnostics in PEMFC stacks by evaluation of local performance and cell impedance analysis. Fuel Cells 2020. https://doi.org/10.1002/fuce.201900193.

[21] Ciureanu M, Roberge R. Electrochemical impedance study of PEM fuel cells. Experimental diagnostics and modeling of air cathodes. J Phys Chem B 2001;105:3531–9. https://doi.org/10.1021/jp003273p.

[22] Shan J, Lin R, Chen X, Diao X. EIS and local resolved current density distribution analysis on effects of MPL on PEMFC performance at varied humidification. Int J Heat Mass Tran 2018;127:1076–83. https://doi.org/10.1016/j.ijheatmasstransfer.2018.08.033.

[23] Halvorsen IJ, Pivac I, Bezmalinović D, Barbir F, Zenith F. Electrochemical low-frequency impedance spectroscopy algorithm for diagnostics of PEM fuel cell degradation. Int J Hydrogen Energy 2020;45:1325–34. https://doi.org/10.1016/j.ijhydene.2019.04.004.

[24] Song C, Tang Y, Zhang JL, Zhang J, Wang H, Shen J, McDermid S, Li J, Kozak P. PEM fuel cell reaction kinetics in the temperature range of 23–120°C. Electrochim Acta 2007;52:2552–61. https://doi.org/10.1016/j.electacta.2006.09.008.

[25] Singh RK, Devivaraprasad R, Kar T, Chakraborty A, Neergat M. Electrochemical impedance spectroscopy of oxygen reduction reaction (ORR) in a rotating disk electrode configuration: effect of ionomer content and carbon-support. J Electrochem Soc 2015;162:F489–98. https://doi.org/10.1149/2.0141506jes.

[26] Paulus UA, Schmidt TJ, Gasteiger HA, Behm RJ. Oxygen reduction on a high-surface area Pt/Vulcan carbon catalyst: a thin-film rotating ring-disk electrode study. J Electroanal Chem 2001;495:134–45. https://doi.org/10.1016/S0022-0728(00)00407-1.

[27] Wagner N, Friedrich KA. Fuel cells – proton-exchange membrane fuel cells | dynamic operational conditions. In: Encyclopedia of electrochemical power sources. Elsevier; 2009. p. 912–30. https://doi.org/10.1016/B978-044452745-5.00239-2.

[28] Moçotéguy P, Ludwig B, Beretta D, Pedersen T. Study of the impact of water management on the performance of PEMFC commercial stacks by impedance spectroscopy. Int J Hydrogen Energy 2020;45:16724–37. https://doi.org/10.1016/j.ijhydene.2020.04.139.

[29] EIS diagnosis for PEM fuel cell performance. In: Electrochemical impedance spectroscopy in PEM fuel cells. London: Springer London; 2010. p. 193–262. https://doi.org/10.1007/978-1-84882-846-9_5.

[30] Asghari S, Mokmeli A, Samavati M. Study of PEM fuel cell performance by electrochemical impedance spectroscopy. Int J Hydrogen Energy 2010;35:9283–90. https://doi.org/10.1016/j.ijhydene.2010.03.069.

[31] O'Rourke J, Ramani M, Arcak M. In situ detection of anode flooding of a PEM fuel cell. Int J Hydrogen Energy 2009;34:6765–70. https://doi.org/10.1016/j.ijhydene.2009.06.029.

[32] Mohammadi Taghiabadi M, Zhiani M. Degradation analysis of dead-ended anode PEM fuel cell at the low and high thermal and pressure conditions. Int J Hydrogen Energy 2019;44:4985–95. https://doi.org/10.1016/j.ijhydene.2019.01.040.

[33] Wagner N. Electrochemical impedance spectroscopy. In: Li H, editor. PEM fuel cell diagnostic tools. CRC Press; 2011. p. 37–70. https://doi.org/10.1201/b11100-5.

[34] Nakajima H, Konomi T, Kitahara T, Tachibana H. Electrochemical impedance parameters for the diagnosis of a polymer electrolyte fuel cell poisoned by carbon monoxide in reformed hydrogen fuel. J Fuel Cell Sci Technol 2008;5:041013. https://doi.org/10.1115/1.2931462.

[35] Rubio MA, Urquia A, Dormido S. Diagnosis of performance degradation phenomena in PEM fuel cells. Int J Hydrogen Energy 2010;35:2586–90. https://doi.org/10.1016/j.ijhydene.2009.03.054.

[36] Qi Z, He C, Kaufman A. Poisoning of proton exchange membrane fuel cell cathode by CO in the anode fuel. Electrochem Solid-State Lett 2001;4:A204. https://doi.org/10.1149/1.1414944.

[37] Qi Z. Effect of CO in the anode fuel on the performance of PEM fuel cell cathode. J Power Sources 2002;111:239–47. https://doi.org/10.1016/S0378-7753(02)00300-2.

[38] Profatilova I, Jacques P-A, Escribano S. Evaluation of parameters accelerating the aging of PEMFCs operating under reformate containing carbon monoxide. J Electrochem Soc 2018;165:F3251–60. https://doi.org/10.1149/2.0281806jes.

[39] Wagner N, Gülzow E. Change of electrochemical impedance spectra (EIS) with time during CO-poisoning of the Pt-anode in a membrane fuel cell. J Power Sources 2004;127:341–7. https://doi.org/10.1016/j.jpowsour.2003.09.031.

[40] Tang Y, Zhang H, Zhong H, Xu Z. In-situ investigation on the CO tolerance of carbon supported Pd–Pt electrocatalysts with low Pt content by electrochemical impedance spectroscopy. Int J Hydrogen Energy 2012;37:2129–36. https://doi.org/10.1016/j.ijhydene.2011.10.104.

[41] Chandesris M, Guetaz L, Schott P, Scohy M, Escribano S. Investigation of degradation heterogeneities in PEMFC stack aged under reformate coupling in situ diagnosis, post-mortem ex situ analyses and multi-physic simulations. J Electrochem Soc 2018;165:F3290–306. https://doi.org/10.1149/2.0321806jes.

[42] Becherif M, Péra M-C, Hissel D, Zheng Z. Determination of the health state of fuel cell vehicle for a clean transportation. J Clean Prod 2018;171:1510–9. https://doi.org/10.1016/j.jclepro.2017.10.072.

[43] Liu D, Lin R, Feng B, Yang Z. Investigation of the effect of cathode stoichiometry of proton exchange membrane fuel cell using localized electrochemical impedance spectroscopy based on print circuit board. Int J Hydrogen Energy 2019;44:7564–73. https://doi.org/10.1016/j.ijhydene.2019.01.095.

[44] Liu D, Lin R, Feng B, Han L, Zhang Y, Ni M, Wu S. Localised electrochemical impedance spectroscopy investigation of polymer electrolyte membrane fuel cells using Print circuit board based interference-free system. Appl Energy 2019;254:113712. https://doi.org/10.1016/j.apenergy.2019.113712.

[45] Suresh R, Swaminathan S, Rengaswamy R. Rapid impedance spectroscopy using dual phase shifted chirp signals for electrochemical applications. Int J Hydrogen Energy 2020;45:10536–48. https://doi.org/10.1016/j.ijhydene.2019.10.031.

[46] Darowicki K, Janicka E, Mielniczek M, Zielinski A, Gawel L, Mitzel J, Hunger J. Implementation of DEIS for reliable fault monitoring and detection in PEMFC single cells and stacks. Electrochim Acta 2018. https://doi.org/10.1016/j.electacta.2018.09.105.

[47] Slepski P, Darowicki K, Janicka E, Lentka G. A complete impedance analysis of electrochemical cells used as energy sources. J Solid State Electrochem 2012;16:3539–49. https://doi.org/10.1007/s10008-012-1825-1.

[48] Slepski P, Janicka E, Darowicki K, Pierozynski B. Impedance monitoring of fuel cell stacks. J Solid State Electrochem 2015;19:929–33. https://doi.org/10.1007/s10008-014-2676-8.

[49] Darowicki K, Janicka E, Slepski P. Study of direct methanol fuel cell process dynamics using dynamic electrochemical impedance spectroscopy. Int J Electrochem Sci 2012;7:12090–7.

[50] Darowicki K, Janicka E, Mielniczek M, Zielinski A, Gawel L, Mitzel J, Hunger J. The influence of dynamic load changes on temporary impedance in hydrogen fuel cells, selection and validation of the electrical equivalent circuit. Appl Energy 2019;251:113396. https://doi.org/10.1016/j.apenergy.2019.113396.

[51] Darowicki K, Gawel L. Impedance measurement and selection of electrochemical equivalent circuit of a working PEM fuel cell cathode. Electrocatalysis 2017;8:235–44. https://doi.org/10.1007/s12678-017-0363-0.

[52] Janicka E, Mielniczek M, Gawel L, Darowicki K, Landowska P. The impact of air humidity on the operation of proton exchange membrane fuel cells determined using dynamic electrochemical impedance spectroscopy. Electrochim Acta 2020:136036. https://doi.org/10.1016/j.electacta.2020.136036.

[53] Wagner N, Schulze M. Change of electrochemical impedance spectra during CO poisoning of the Pt and Pt–Ru anodes in a membrane fuel cell (PEFC). Electrochim Acta 2003;48:3899–907. https://doi.org/10.1016/S0013-4686(03)00528-0.

[54] Min Jeffery, Kim Jung. Electrochemical analysis for demonstrating CO tolerance of catalysts in polymer electrolyte membrane fuel cells. Nanomaterials 2019;9:1425. https://doi.org/10.3390/nano9101425.

[55] Ciureanu M, Roberge R. Electrochemical impedance study of PEM fuel cells. Experimental diagnostics and modeling of air cathodes. J Phys Chem B 2001;105:3531–9. https://doi.org/10.1021/jp003273p.

[56] Orazem ME, Tribollet B. Electrochemical impedance spectroscopy: orazem/electrochemical. Hoboken, NJ, USA: John Wiley & Sons, Inc.; 2008. https://doi.org/10.1002/9780470381588.ch19.

[57] Darowicki K. Theoretical description of the measuring method of instantaneous impedance spectra. J Electroanal Chem 2000;486:101–5. https://doi.org/10.1016/S0022-0728(00)00110-8.

[58] Darowicki K, Ślepski P. Dynamic electrochemical impedance spectroscopy of the first order electrode reaction. J Electroanal Chem 2003;547:1–8. https://doi.org/10.1016/S0022-0728(03)00154-2.

[59] Darowicki K, Ślepski P. Influence of the analyzing window on electrode impedance measurement by the continuous frequency scanning method. J Electroanal Chem 2002;533:25–31. https://doi.org/10.1016/S0022-0728(02)01085-9.

[60] Darowicki K, Orlikowski J, Lentka G. Instantaneous impedance spectra of a non-stationary model electrical system. J Electroanal Chem 2000;486:106–10. https://doi.org/10.1016/S0022-0728(00)00111-X.

[61] Armstrong RD, Firman RE. Impedance plane display of a reaction with a solution soluble intermediate. J Electroanal Chem Interfacial Electrochem 1973;45:3–10. https://doi.org/10.1016/S0022-0728(73)80003-8.

[62] Armstrong RD, Henderson M. Impedance plane display of a reaction with an adsorbed intermediate. J Electroanal Chem Interfacial Electrochem 1972;39:81–90. https://doi.org/10.1016/S0022-0728(72)80477-7.

[63] Kucernak AR, Zalitis C. General models for the electrochemical hydrogen oxidation and hydrogen evolution reactions: theoretical derivation and experimental results under near mass-transport free conditions. J Phys Chem C 2016;120:10721–45. https://doi.org/10.1021/acs.jpcc.6b00011.

[64] Wang JX, Springer TE, Adzic RR. Dual-pathway kinetic equation for the hydrogen oxidation reaction on Pt electrodes. J Electrochem Soc 2006;153:A1732. https://doi.org/10.1149/1.2218756.

[65] Wang JiaX, Springer TE, Liu P, Shao M, Adzic RR. Hydrogen oxidation reaction on Pt in acidic media: adsorption isotherm and activation free energies. J Phys Chem C 2007;111:12425–33. https://doi.org/10.1021/jp073400i.